Disruption Scenarios, their Mitigation and Operation Window in ITER

M. Shimada[1], M. Sugihara[1], H. Fujieda[2], Yu. Gribov[1], K. Ioki[3], Y. Kawano[2], R. Khayrutdinov[4], V. Lukash[5], J. Ohmori[2]

[1] *ITER IT, Naka JWS, Naka, Ibaraki, Japan,* [2] *JAEA, Naka, Ibaraki, Japan,*
[3] *ITER IT, Garching JWS, Garching, Germany,* [4] *TRINITI, Russian Federation,*
[5] *Kurchatov Institute, Russian Federation,*
e-mail address of the main author; michiya.shimada@iter.org

Abstract The impacts of plasma disruptions on ITER have been investigated in detail to confirm the robustness of the design of the machine to the potential consequential loads. The loads include both electro-magnetic (EM) and heat loads on the in-vessel components and the vacuum vessel (VV). Several representative disruption scenarios are specified based on newly derived physics guidelines for the shortest current quench time as well as the maximum product of halo current fraction and toroidal peaking factor arising from disruptions in ITER. Disruption simulations with the DINA code and electromagnetic load (EM) analyses with a 3D finite element method (FEM) code are performed for these scenarios. Some margins are confirmed in the EM load on in-vessel components due to induced eddy and halo currents for these representative scenarios. However, the margins are not very large. The heat load on various parts of the first wall due to vertical movements and thermal quench (TQ) is calculated based on the database of heat deposition during disruptions and simulation results with the DINA code. It is found that the beryllium wall will not melt during the vertical movement. Melting is anticipated due to TQ after vertical movement, though its impact can be mitigated by implementing a reliable detection and mitigation system, e.g., massive gas injection. Some melting is anticipated at major disruptions (MD). At least several tens of unmitigated disruptions must be considered even if an advanced prediction/mitigation system is implemented. With these unmitigated disruptions, the loss of beryllium layer is expected to be within $\approx$ *20 μm*/event out of *10 mm* thick beryllium first wall.

1. Introduction

Detailed examinations of EM and heat loads under various disruption conditions expected in ITER are essential to check the robustness of the design against the potential consequential loads. Robustness of the VV and large in-vessel components, such as the blanket modules (BM) and divertor cassette, are particularly important since they are directly linked with the protection of the machine against mechanical damage. A reasonable margin against the mechanical stress must be reserved for these representative scenarios since the disruption prediction/mitigation system cannot be expected to be 100% reliable and some disruptions will unavoidably occur. On the other hand, the prediction/mitigation system will be very effective for reducing the damage of the plasma facing components (PFC) due to the thermal load during TQ and vertical displacement event (VDEs).

For this purpose, a proper specification of representative disruption scenarios based on detailed assessment of the database is essential [1]. Of particular importance for the assessment of EM loads are the shortest current quench time, and the maximum product of halo current fraction ($I_{h,max}/I_{p0}$) and toroidal peaking factor (*TPF*), $f_h \equiv (I_{h,max}/I_{p0}) \times TPF$. To estimate the heat load it is necessary to know the thermal energy content at the TQ, the energy deposition width and time duration. The details of the plasma behavior are also important in order to evaluate the heat load during VDEs. The database on the heat load is still limited.

Among the mitigation techniques so far proposed, the massive noble gas injection technique seems to be the most promising [2, 3]. This technique provides a sound basis for the mitigation of heat load. It is important to assess the mitigation success or missed rate in ITER with these techniques. Here, mitigation success rates are defined as the ratio of the number of disruptive discharges which are successfully mitigated to the total number of disruptive discharges. This assessment can be performed by using sophisticated disruption prediction methods, such as a neural network system [4], applied to the possible mitigation

scenarios. The success rate strongly depends on the response time, which is closely linked to the gas pressure and the resulting force on the gas inlet valve through the response speed of the gas injection/penetration [5].

In this paper, we first simulate representative disruption scenarios with the disruption simulation code DINA based on the recently derived guideline for the shortest current quench time. We then evaluate the EM load on BMs and VV due to the induced eddy and halo current using the maximum f_h expected in ITER from database analyses. The heat loads on various parts of the BMs and divertor during VDEs and the TQ are evaluated for these scenarios. An application of a neural network prediction technique is made to assess the mitigation success rate and the resulting lifetime of the first wall is estimated.

2. Representative Disruption Scenarios and the Associated EM Load

The origin of the most critical EM load is different for different components. For the VV, the vertical force due to the induced halo current is the most critical. VDEs with a slow current quench, where the halo current is expected to be the largest, are of major concern for the VV. As for the BMs, the EM load due to the induced eddy current is dominant, while the halo current also contributes to some extent. Thus, the MDs and VDEs with the fastest current quench are the most important for BMs. In this way, the guidelines for the fastest current quench and the halo current are the most important for the evaluation of the EM loads on BMs and the VV.

Since the previous International Disruption Database (IDD) prepared for the ITER physics basis (IPB) [1], a new IDD has been initiated with a particular emphasis on the fastest current quench for each machine [6, 7]. In contrast to the previous evaluation, the quench time Δt is evaluated from the average quench rate between *80%* and *20%* of the initial plasma current I_{p0} for all machines. From this database, it is recommended to use *1 ms/m*^{2} as the guideline for the fastest current quench time normalized by the poloidal cross-section area ($\Delta t/S$) for *60 %* current quench [8]. This corresponds to the full current quench (*100-0%*) time of *36* ms for ITER when a linear waveform is assumed. For the purpose of the EM load analysis, we also employ the exponential waveform of the current quench as in our previous papers [5, 9, 10]. Namely, we use the exponential curve, which passes through *80%* and *20%* of I_{p0} for the shortest linear waveform expected in ITER. This provides a time constant of $\tau \approx$ *16 ms* in ITER. Experimental data for *TPF* as a function of maximum poloidal halo fraction $I_{h,max}/I_{p0}$ have been summarized in IPB [1]. Data have been updated with addition of further experimental data from MAST, JET and JT-60U [11, 12, 13]. This database indicates that the maximum $f_h \approx 0.7$. A large poloidal halo current is driven when the plasma current decays slowly, since the edge safety factor reduces significantly under this condition. In the ITER application, the maximum $I_{h,max}/I_{p0}$ is evaluated to be ≈ 0.44 in VDE with a slow current quench with a simulation code, as shown later. Then, the *TPF* is evaluated from $0.7/(I_{h,max}/I_{p0})$ and the resulting *TPF* (≈ 1.6) is also applied to disruptions and VDEs with the fast current quench, which contributes to the EM load on BMs to some extent.

Based on these guidelines, several representative disruption scenarios have been prepared for the EM load analyses. They include MDs with fast current quench, upward and downward VDEs with fast and slow current quenches. Numerical simulations are performed with the DINA code [14] for these representative scenarios to simulate the detailed plasma behavior during disruptions. The DINA code solves the evolution of 2D plasma equilibrium on closed and open magnetic surfaces together with external circuits (PF coils and surrounding conducting structures). Details of ITER modeling with the DINA code are

described in [5]. Induced eddy currents on these surrounding structures are calculated with a 3D finite element method (FEM) code using the time behavior of the toroidal current density of the plasma column evaluated with the DINA code. EM load analyses are performed using these induced eddy currents. The BMs are connected to the VV through key structures and flexible supports. The key structure restrains the displacement of the module parallel to the VV wall reacting to the poloidal and toroidal forces and the radial moment (*Mr*). The flexible support reacts to the loads in the radial direction while being compliant in the other directions. Consequently, vertical (poloidal) forces (*Fp*) both due to eddy and halo currents are superimposed on the key. Actually, this force is the most difficult to resist because of space limitation at the key structure. Thus, in this section, we will discuss the EM load on the key structure for various representative scenarios. Figure 1 shows the time evolution of plasma current, vertical position and poloidal halo current for a downward VDE with a linear 36 ms current quench time. Figure 2 shows four time slices of Last Closed Flux Surface (LCFS; red) and halo boundaries (green) for this case at (a), (b), (c) and (d) in Fig. 1. The VDE starts at $t = 0$. Plasma moves downward and a TQ occurs when the surface q value reaches *1.5* [15] at $t = 670$ *ms*. Figures 3 and 4 show the corresponding time behaviors for an upward VDE with an exponential time constant of *16 ms*.

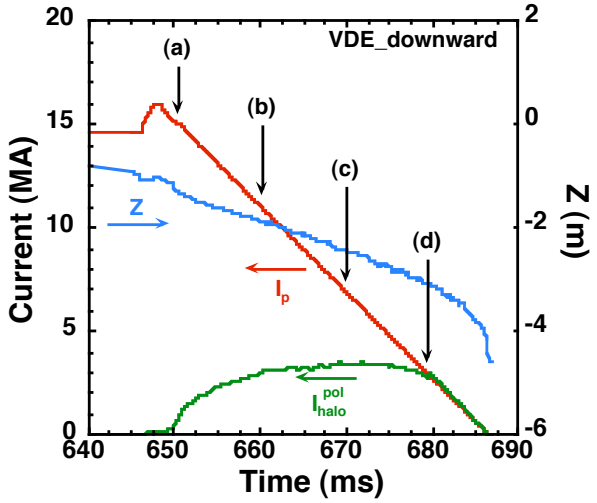

Fig. 1 Time evolutions of plasma current, vertical position and poloidal halo current for downward VDE with linear 36 ms quench.

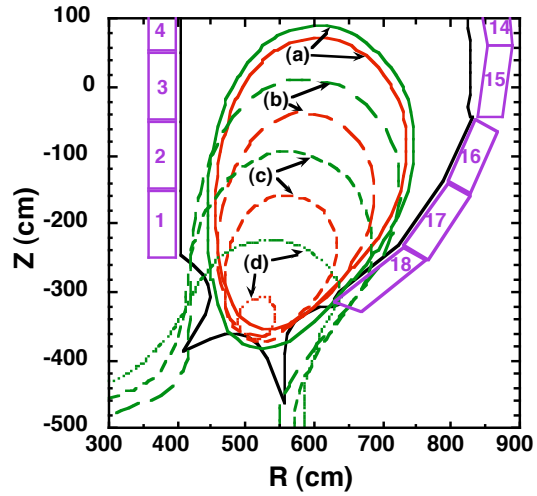

Fig. 2 Time evolution of plasma (LCFS) and halo boundaries for the case of Fig. 1 at four time points (a), (b), (c) and (d).

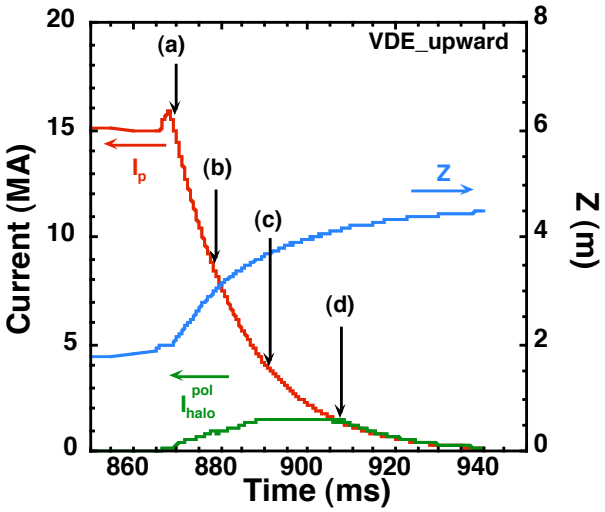

Fig. 3 Time evolutions of plasma current, vertical position and poloidal halo current for upward VDE with exponential waveform of 16 ms time constant.

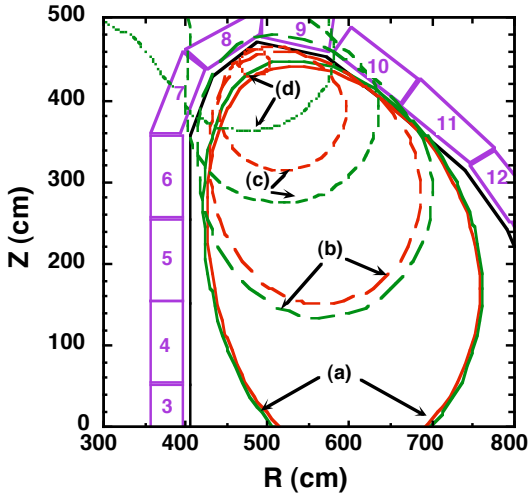

Fig. 4 Time evolution of plasma (LCFS) and halo boundaries for the case of Fig. 3 at four time points (a), (b), (c) and (d).

Figures 5 and 6 show the maximum poloidal (vertical) forces *Fp* due to eddy and halo currents on #1-10 BMs (Fig. 5) and #11-18 BMs (Fig. 6) for representative scenarios of MD (MD_lin and MD_exp) and upward/downward VDEs (VDE_UP_lin, VDE_UP_exp, VDE_DW_lin and VDE_DW_exp) with a fast current quench (*36 ms* quench time for linearwaveform and *16 ms* time constant for exponential waveform), respectively. The *TPF=1.6* is used to evaluate the local maximum force due to the halo current. The time evolution of the halo current path is obtained by the DINA code calculation, and the possible maximum fraction of the halo current flowing into each BM is assumed. For instance, $f_1 \equiv I_{halo}(Nr.1)/I_{halo,total}=0.5$ is assumed during the whole current quench phase to keep some margin against the uncertainty of the plasma behavior. The numbers of BMs with high *Fp* are shown in the figure. The solid line shows the allowable *Fp* due to the induced eddy current as a function of *Fp* due to the induced halo current. This includes the effect of dynamic factor of *1.5* due to the dynamical motion of BM at the onset of *Fp*. The dashed line shows the allowable *Fp* when the event is very rare (1-2 during the whole life), which is *20%* higher than the solid line (criterion by American Society of Mechanical Engineers). It is seen from Figs 5 and 6 that EM loads on all BMs are within the allowable limit for the representative disruption scenarios investigated. Since the present margins are not large, further efforts to identify the margins more credibly from the physics side and to increase the margins from the engineering side are highly desirable to further increase the robustness of the machine. Of particular importance from the physics side, is further development of the models of plasma behaviors including halo fraction, toroidal peaking factor and width of halo current region. Since the plasma movement is very slow during a VDE, it appears to be feasible to decrease the number of unmitigated VDE to 1-2 times during the whole life by constructing a reliable position detection system and disruption mitigation system.

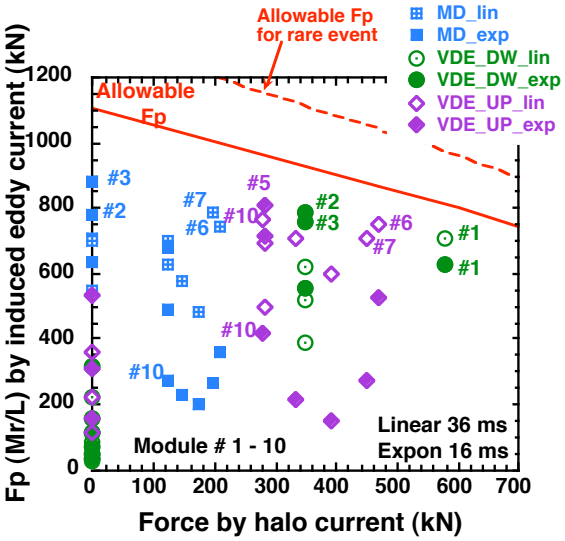

Fig. 5 Maximum Fp due to eddy and halo currents on #1-10 BMs for representative scenarios.

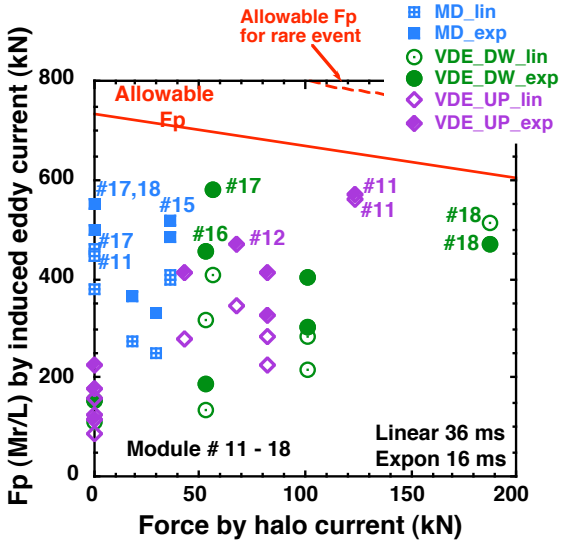

Fig. 6 Maximum Fp due to eddy and halo currents on #11-18 BMs for representative scenarios.

3. Heat Load on PFC during VDEs and TQ

The heat load on PFCs during VDEs and the TQ can make a large impact on their lifetimes. In particular, the impact on beryllium first wall can be very large, since its melting

Table 1 Assumption taken from [16] used for the estimation of heat load on beryllium first wall

Energy release at TQ (relative to peak stored energy W_{peak})	*(0.5-1.0) W_{peak}*
Expansion factor of heat load width from the steady heat load width λss	*(5-10)*
Time duration of heat deposition on divertor/wall	*(1.5-3) ms*

temperature is rather low. Unfortunately, the database of heat load during the TQ is very limited. The most systematic database so far available is in [16]. In this paper, we will use this database to estimate the heat load on the beryllium first wall during VDEs and TQs. Table 1summarizes assumptions taken from this database.

3.1 Heat Load during Major Disruptions

In the case of MDs, the largest heat load on the beryllium first wall is that on the upper wall, since half of the heat flux across the second separatrix will be deposited. Figure 7 shows the flux surfaces near the upper wall from the equilibrium calculation. Fig. 8 shows the peak heat load density on the upper wall during the TQ of MDs for reference (green) and possible worst (red) equilibrium configurations (it is assumed W_{peak} =*1MJ* and λss =*5 mm*). Upper and lower bound correspond to the expansion factor of λss (*5* corresponds to lower and *10* to upper). Table 2 summarizes the peak heat loads for two cases of W_{peak} (*175 MJ* and *350 MJ*). The range corresponds to the expansion factors *5* to left and *10* to right. From Table 2, it is seen that the measure of energy load ε ($MJ/m^2/s^{1/2}$) is in the range of *8.2-75* $MJ/m^2/s^{1/2}$ for the deposition time duration of *1.5-3 ms*. The criterion for melting of beryllium is ≈*20* $MJ/m^2/s^{1/2}$ and, thus, melting of beryllium is expected in many MD cases. The loss of beryllium thickness can be estimated as ≈*20 μm*/event for *1* MJ/m^2 even if the whole melt layer is lost based on calculations including the vapor shielding effect [1]. In fact, the missed rate of prediction cannot be decreased below several % even with the most advanced algorithm of neural network [4]. In particular, for high beta plasmas, it is shown that the missed rate is further increased up to ≈*20%* [17, 18]. Thus, several tens of unmitigated TQs must be expected out of ≈*3000* MDs (≈10 % of $3x10^4$ total shots) in ITER.

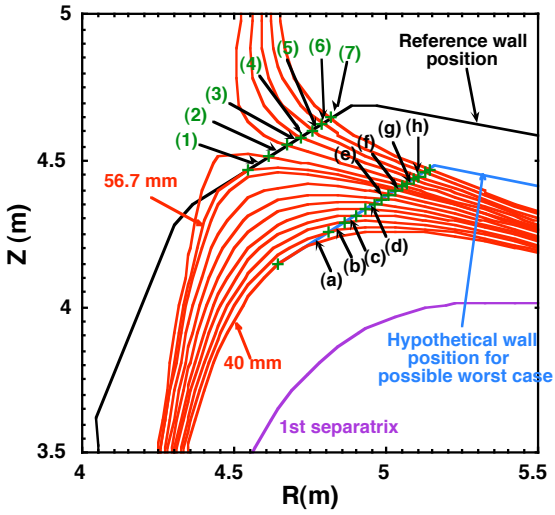

Fig. 7 Flux surfaces near the upper wall for reference equilibrium. Wall position for possible worst case is shown in blue.

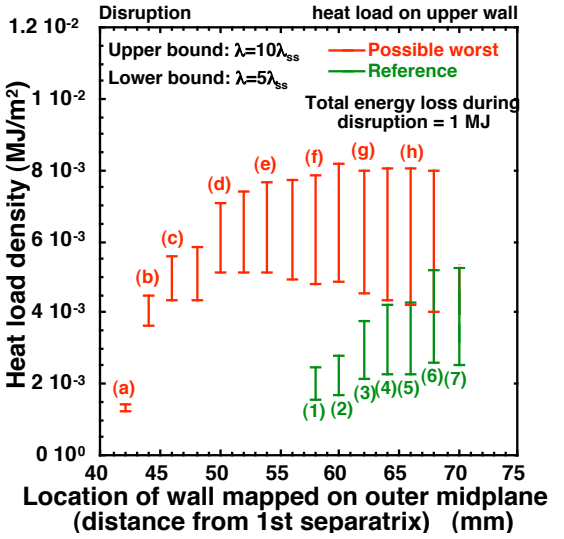

Fig. 8 Heat load density on upper first wall during TQ for reference (green) and possible worst (red) equilibrium configurations.

Table 2 Peak heat load density on the upper wall during TQ of MD.

Energy loss / disruption Case and peak location	*175 MJ*	*350 MJ*
Reference : peak location (6) – (8) (MJ/m^2) (Fig.8)	*0.45 – 0.92*	*0.9 – 1.84*
Possible worst : peak location (f) - (g) (MJ/m^2) (Fig.8)	*0.9 – 1.44*	*1.8 – 2.9*

3.2 Heat Load during VDEs

In the case of VDEs, the heat load on the beryllium first wall during two phases must

be properly assessed. The first phase is during the vertical movement of the hot plasma limited by the first wall. The second phase is during the TQ subsequently triggered after the vertical movement. Both upper and lower first walls must be examined, since upward and downward VDEs will occur with an equal probability.

Figure 9 shows equilibrium configurations during upward VDE at *600 ms* (early phase of plasma touching the upper wall) and at *865 ms* (just before TQ at *q=1.5*). The numbers on the wall are indicators of the position. The insert in Fig. 9 shows the time evolution of plasma current and edge safety factor. Fig. 10 shows ε at each wall position during the vertical movement (*550-865 ms*) for three different λss. It is assumed that after touching the wall, the plasma transits back to the L mode and the heat flow across the LCFS is *200 MW* (more than twice of the H mode phase). After L mode transition, λss is assumed wider than that of H mode phase, and thus, *≈1 cm* is assumed as a typical value in this paper. Detailed plasma magnetic configuration and incident angle of the field line with the first wall are taken into account in Fig. 10. It is seen that ε is well below the critical value for the melting of beryllium. Thus, melting will not occur during the vertical movement even if there is some asymmetry of heat load between electron and ion sides or by misalignment. At some moment during the vertical movement, a TQ will occur. Figure 11 shows ε at each wall position for TQ occurrence times at *600 ms* (green dotted line) and *865 ms* (red solid line). It is assumed that a half of W_{peak} (*175MJ*) is released at TQ with a deposition width of *5 cm* and a time duration of the energy deposition of *1.5 ms*. Triangles show the maximum values if TQ occurs at arbitrary time moment during *570 ms* and *865 ms*. It is seen from Fig. 11 that a wide region of the wall receives the heat in the early phase while ε exceeds the critical value in limited regions. In the later phase, ε significantly exceeds the critical value in some regions, and a loss of *≈30 μm*/event is anticipated. Of particular concern is the

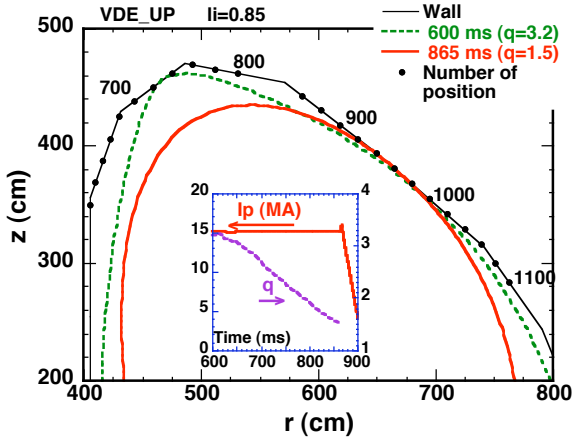

Fig. 9 Equilibrium configurations at 600 ms (early phase of plasma touching the upper wall) and at 865 ms (just before TQ at q=1.5). Insert shows time evolution of plasma current and safety factor.

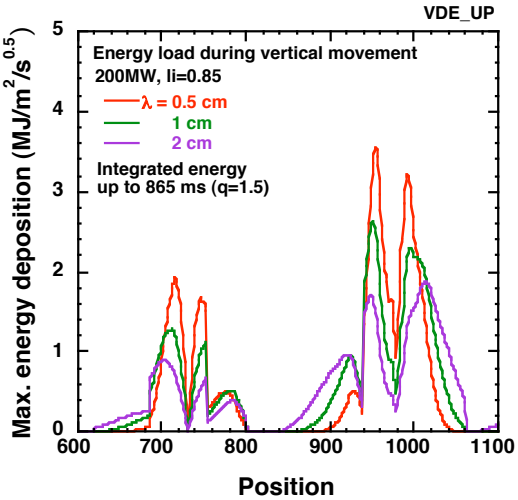

Fig. 10 Measure of energy load ε at each wall position during vertical movement (570-865 ms) for three different λss.

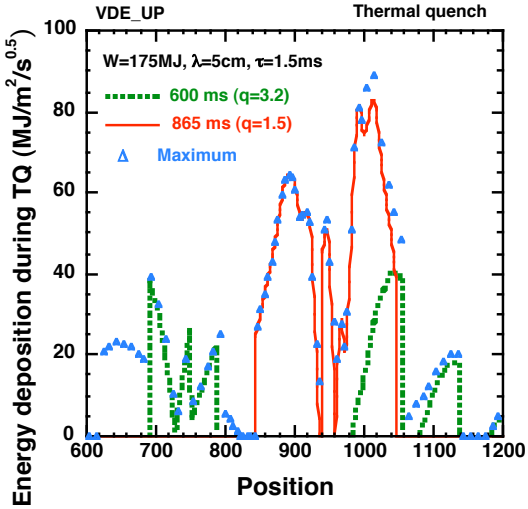

Fig. 11 Measure of energy load for each wall position for two cases of TQ occurrence times, i.e., at 600 ms (green) and 865 ms (red).

energy load on the upper wall (position from *720 to 760)*, where a loss of ≈*20 μm*/event is expected by MDs. However, the additional loss by VDEs is small, since the number of occurrence of VDE will be made very infrequent due to the VDE detection system in ITER.

Figure 12 shows equilibrium configurations during a downward VDE at *600 ms* (early phase; *q=2.1*) and at *645 ms* (just before TQ; *q=1.5*). Fig. 13 shows ε at each wall position after the plasma touches the wall during the vertical movement (*550-645 ms*) for three different widths of heat flux at the mid-plane. The heat flow across the LCFS is *200 MW*. Generally ε is larger than the upward VDE case due to the larger intersecting angle between the flux surfaces and the wall, especially for the baffle region. However, ε is below the critical value for melting both for the beryllium first wall and tungsten baffle during this phase. Figure 14 shows ε during the TQ at *600 ms* (green) and *645 ms* (red). Triangles show the maximum values if the TQ occurs at an arbitrary time during *550 ms* and *645 ms*. Although ε exceeds the critical value, it is somewhat smaller on the beryllium first wall than upward VDE case. A much larger ε is anticipated and it significantly exceeds the critical value (*60* $MJ/m^2/s^{1/2}$ for the tungsten baffle region), and the loss of tungsten baffle is ≈*60 μm*/event. These evaluations conclude that the beryllium first wall will not melt during the vertical movement even after the plasma touches the wall both for upward and downward VDEs. Melting is, however, anticipated during the TQ. It is naturally expected that the lifetime can be substantially prolonged if mitigation can be triggered before the occurrence of TQ during most of VDEs. There should be high chance of realising such a prediction/mitigation system in ITER with, for example, massive gas injection, since it takes more than *0.5 s* before the plasma first contacts the wall during VDEs in ITER, during which the plasma movement can be detected.

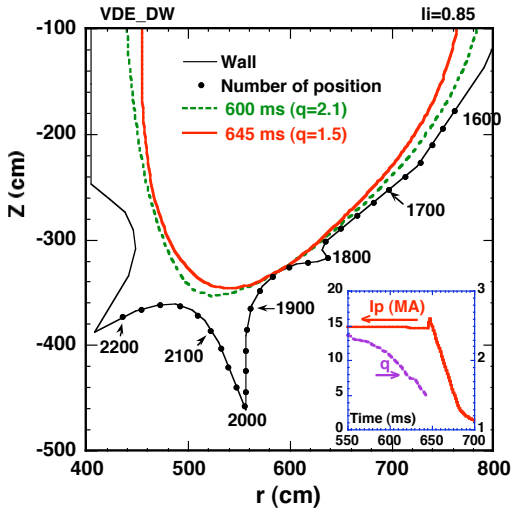

Fig. 12 Equilibrium configurations at 600 ms (q=2.1) and at 645 ms (just before TQ at q=1.5). Insert shows time evolution of plasma current and safety factor.

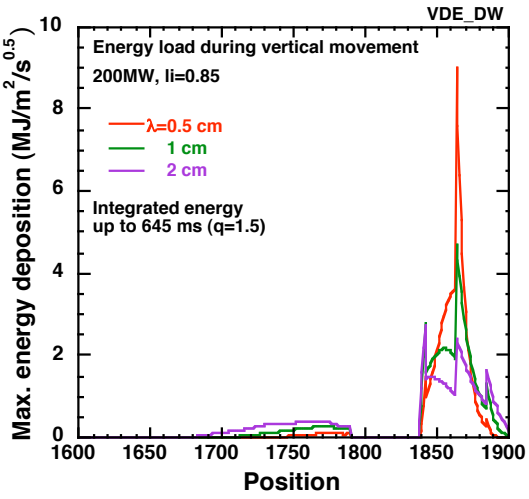

Fig. 13 Measure of energy load at each wall position during the vertical movement (550-645 ms) for three different widths of heat flux.

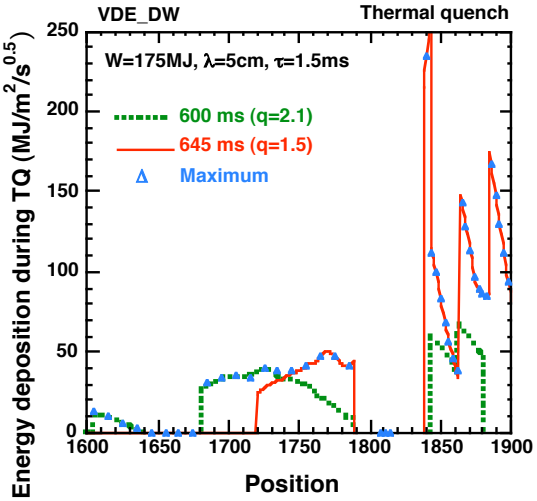

Fig. 14 Measure of energy load at two different time moment of the occurrence of TQ, 600 ms (green) and 645 ms (red).

4. Conclusions

Several representative disruption scenarios are specified and disruption simulations are performed with the DINA code and EM load analyses with the 3D FEM code for these scenarios based on newly derived physics guidelines for the shortest current quench time and their waveforms ($\Delta t \approx 36$ *ms* linear and $\tau \approx 16$ *ms* exponential waveforms), as well as the maximum product of halo current fraction and toroidal peaking factor (maximum $f_h \approx 0.7$) expected in ITER. Although some margins are confirmed in the EM loads due to induced eddy and halo currents on the in-vessel components for all of the representative scenarios, further efforts both from the physics and engineering sides are needed to enlarge the margins.

The heat load on various parts of the first wall due to vertical movements and TQs is calculated based on the database of heat deposition during disruptions and simulation results with the DINA code. It is concluded that melting of beryllium wall during vertical movement will not occur. Melting is anticipated at the TQ during a VDE, though its impact could be reduced substantially by implementing a reliable detection and mitigation system, e.g., massive gas injection. Latest experiments show that radiative heat load on the first wall due to the massive gas injection will not be so localized and ε is marginally below the critical value for melting [3]. More severe melting is anticipated due to MDs, for which at least several tens of unmitigated disruptions must be considered even if an advanced prediction/mitigation system is implemented. With these unmitigated MDs the loss of beryllium layer is expected to be ≈*20 μm*/event.

Acknowledgements

This report was prepared as an account of work undertaken within the framework of ITER Transitional Arrangements (ITA). These are conducted by the Participants: the European Atomic Energy Community, India, Japan, the People's Republic of China, the Republic of Korea, the Russian Federation, and the United States of America, under the auspices of the International Atomic Energy Agency. The views and opinions expressed herein do not necessarily reflect those of the Participants to the ITA, the IAEA or any agency thereof. Dissemination of the information in this paper is governed by the applicable terms of the former ITER EDA Agreement.

References

[1] ITER Physics Basis, Nucl. Fusion **39** (1999) 2137.
[2] Whyte, D., J. Nucl. Material. **313-316** (2003) 1239.
[3] Hollmann, E.M., et al., Proc. 20th IAEA FEC, Vilamoura (2004) IT/EX/10-6Ra.
[4] Yoshino, R., Nucl. Fusion **43** (2003) 1771.
[5] Sugihara, M., et al., Proc. 20th IAEA FEC, Vilamoura (2004) IT/P3-29.
[6] Hyatt, A., et al., 47th meeting of APS Division of Plasma Physics, Denver (2005), CP1.28.
[7] Riccardo, V., et al., Plasma Phys. Control. Fusion **47** (2005) 117.
[8] Wesley, J., et al., "Disruption Characterization and Database Activities for ITER", this conference, IT/P1-21.
[9] Sugihara, M., et al., J. Plasma Fusion Science **79** (2003) 706.
[10] Sugihara, M., et al., 30th EPS, St. Petersburg (2003), P-2.139.
[11] Riccardo, V., Plasma Phys. Control. Fusion **45** (2003) A269.
[12] Riccardo, V., Plasma Phys. Control. Fusion **46** (2004) 925.
[13] Neyatani, Y., et al Nucl. Fusion **39** (1999) 559.
[14] Khayrutdinov, R.R. et al, J. Comp. Physics **109** (1993) 193.
[15] Sugihara, M., et al., Plasma Phys. Control. Fusion **46** (2004) 1581.
[16] Loarte, A., et al., Proc. 20th IAEA FEC, Vilamoura (2004) IT/P3-34.
[17] Wroblewski, D., et al., Nucl. Fusion **37** (1997) 725.
[18] Yoshino, R., Nucl. Fusion **45** (2005) 1232.